Geomechanics and Engineering, *Vol. 35, No. 3 (2023) 307-313*
https://doi.org/10.12989/gae.2023.35.3.307

Mathematical model for rock-soil slope stability based on numerical solution

Shan Hua[1], Maryam Shokravi[2] and S.S. Wang*[1]

[1]*School of Earth Science and Resources, Chang'an University, Xi'an, Shaanxi,710064, China*
[2]*Department of Education, Mehrab High School, Saveh, Iran*
[3]*Faculty of Applied Sciences, Malaysia University, Malaysia*

(*Received April 26, 2023, Revised October 19, 2023, Accepted October 23, 2023*)

Abstract. In this article, a two-phase random medium is assumed for geometric interfaces between rock and soil based on Gaussian field and piezoelectric layer. The structure is modeled by thick plate mathematically and the numerical model is applied to approximation the statistical features of the safety. The elastic medium is simulated with two parameters of spring and shear. The structure is modelled by sinusoidal shear deformation theory (SSDT) and by utilizing the energy method, the final governing equations are derived. Using differential quadrature method, the motion equations are solved for obtaining the failure mode of the rock-soil slope. The results show that the safety factor of rock is dependent to the soil volume faction significantly. Numerical results show that as the structure length is increased, the safety load is decreased. In addition, the application of negative voltage improves the safety of the structure.

Keywords: mathematical model; numerical method; rock-soil; stability

1. Introduction

Nanocomposite structures are made from a matrix reinforced with nanoparticles to improve the properties of the material. Recently, the properties of nanocomposite structures have encouraged researchers to investigate these materials. These structures have many applications such as producing batteries with greater power output, speeding up the healing process for broken bones, producing structural components with a high strength-to-weight ratio, and other applications.

Stability analysis of composite structures has been presented by many researchers. Bending and local stability of a nanocomposite beam reinforced by a single-walled carbon nanotube (SWCNT) were studied by Vodenitcharova and Zhang (2006) based on the Airy stress-function method. Stability analysis of nanocomposite Timoshenko beams reinforced by SWCNTs resting on an elastic foundation was investigated by Yas and Samadi (2012) using the generalized differential quadrature method (GDQM). Kolahchi *et al*. (2015) investigated nonlocal nonlinear stability analysis of temperature-dependent microplates reinforced with FG-SWCNT resting on an elastic matrix as orthotropic temperature-dependent elastomeric medium. Based on harmonic differential quadrature (HDQ), Mehri *et al*. (2016) analyzed stability and vibration responses of a composite truncated conical shell with embedded SWCNTs subjected to an external pressure and axial compression simultaneously. Stability and vibration analysis of a cantilever functionally graded (FG) beam reinforced with carbon nanotube (CNT) were presented by Nejati *et al.* (2016). In this paper, an equivalent continuum model based on the Eshelby–Mori–Tanaka approach was obtained. Based on DQM and Bolotin's method, Kolahchi *et al.* (2016a, b) investigated nonlinear dynamic stability analysis of embedded temperature-dependent viscoelastic plates reinforced by SWCNTs. Mosharrafian and Kolahchi (2016) presented stability analysis of a classical piezoelectric polymeric cylindrical shell reinforced by armchair double-walled boron nitride nanotubes (DWBNNTs). The free vibration and linearized stability analysis of laminated composite plates were studied using the Isogeometric approach (IGA) and Carrera's Unified Formulation (CUF) (Alesadi *et al.* 2017). Yang *et al*. (2017) studied stability and poststability behavior of functionally graded multilayer nanocomposite beams reinforced with a low content of graphene platelets (GPLs) resting on an elastic foundation.

It was assumed that GPLs are randomly oriented and uniformly dispersed in each individual GPL-reinforced composite (GPLRC) layer with its weight fraction varying layerwise along the thickness direction. Zamanian *et al.* (2017) investigated stability of embedded straight beams reinforced with silicon dioxide (SiO2) nanoparticles based on Euler-Bernoulli and Timoshenko beam models. The nonlinear stability of straight beams armed with SWCNTs resting on a foundation was investigated by Bilouei et al. (2016) using DQM. Khelifa *et al.* (2018) presented a multi-layer finite element for stability and free vibration analyses of laminated beams based on a higher-order layer-wise theory. The influence of the initial lateral (sweep) shape and the cross-sectional twist imperfection on the lateral torsional stability (LTB) response of doubly-symmetric steel I-beams was investigated by Benahmed *et al.* (2019). Post-stability of a cut-out plate reinforced through carbon nanotubes (CNTs) resting on an elastic foundation was studied by Motezaker and Eyvazian (2022a). In another

*Corresponding author, Professor
E-mail: wang.lucb@gmail.com

ISSN: 2005-307X (Print), 2092-6219 (Online)

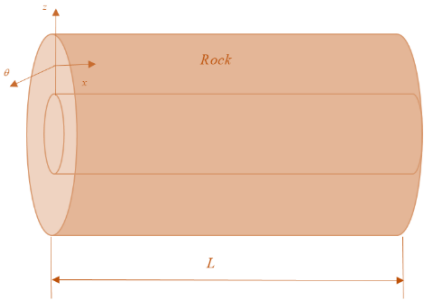

(a)

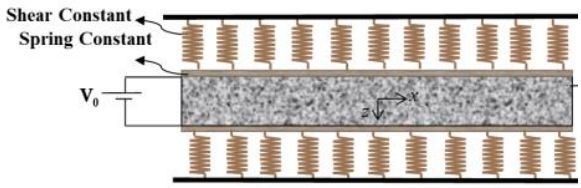

(b)

Fig. 1 The schematic view of the (a) soil-rock model and (b) a smart beam

work by the same authors, stability and optimization of a nanocomposite beam was studied by Motezaker and Eyvazian (2022b). Eltaher and Mohamed (2022) presented a comprehensive model to study static stability stability and associated mode-shapes of higher shear deformation theories of sandwich laminated composite beam under the compression of varying axial load function.

However, to date, no research about the stability of smart nanocomposite roch-soil beam with mathematical models has been found in the literature. The novelty of conducting a stability analysis in concrete nanocomposite smart beams lies in the integration of nanotechnology and smart materials into traditional concrete structures, the development of specialized mathematical models and advanced numerical simulations, and improved sustainability in civil engineering applications. For the first time, the stability analysis of embedded smart beams under the stability constraint is presented in this present work. The SSDT is used for modeling the structure, and the corresponded governing equations are derived by energy method and Hamilton's principal. Using DQM, the stability load of the structure is calculated. The effects of the axial forces, applied voltage, beam length and thickness, spring constant, and shear constant of foundation on the stability load are studied.

2. Formulation

A rock-soil model is shown in Fig. 1(a). This is modelled by smart beam with a length of L and cross section of $b\times h$ is shown in Fig. 1(b), where the structure is subjected to external applied voltage in the thickness direction and surrounded by elastic foundation.

Using Timoshenko model, the displacement field can be written as (Thai and Vo 2012)

$$u_1(x,z,t)=u(x,t)+z\,\psi(x,t)\,, \tag{1}$$

$$u_2(x,z,t)=0\,, \tag{2}$$

$$u_3(x,z,t)=w(x,t)\,, \tag{3}$$

where u_1, u_2 and u_3 are the displacements in the axial, transverse and thickness directions, respectively; u and w are the mid-plane displacements in the axial and thickness directions, respectively; ψ represents the rotation of the cross section about the y axis. Using Eqs. (1) to (3), the nonlinear strain-displacement relations based on the Von - Karman theory are as follows

$$\varepsilon_{xx}=\frac{\partial u}{\partial x}+\frac{1}{2}\left(\frac{\partial w}{\partial x}\right)^2+z\,\frac{\partial \psi}{\partial x}, \tag{4}$$

$$\varepsilon_{xz}=\psi+\frac{\partial w}{\partial x}, \tag{5}$$

where ε_{xx} is normal strain and ε_{xz} is shear strain. In piezoelectric materials, stress (σ) and strain (ε) from the side with an electrical displacement (D) and electric field (E) from the electrostatic side can be coupled as follows (Kolahchi *et al*. 2016a)

$$\begin{bmatrix}\sigma_{xx}\\ \sigma_{yy}\\ \sigma_{zz}\\ \tau_{yz}\\ \tau_{xz}\\ \tau_{xy}\end{bmatrix}=\begin{bmatrix}Q_{11}&Q_{12}&Q_{13}&0&0&0\\ Q_{12}&Q_{22}&Q_{23}&0&0&0\\ Q_{13}&Q_{23}&Q_{33}&0&0&0\\ 0&0&0&Q_{44}&0&0\\ 0&0&0&0&Q_{55}&0\\ 0&0&0&0&0&Q_{66}\end{bmatrix}\begin{Bmatrix}\varepsilon_{xx}\\ \varepsilon_{yy}\\ \varepsilon_{zz}\\ \gamma_{yz}\\ \gamma_{xz}\\ \gamma_{xy}\end{Bmatrix}-\begin{bmatrix}0&0&e_{31}\\ 0&0&e_{32}\\ 0&0&e_{33}\\ 0&e_{24}&0\\ e_{15}&0&0\\ 0&0&0\end{bmatrix}\begin{Bmatrix}E_x\\ E_y\\ E_z\end{Bmatrix}, \tag{6}$$

$$\begin{bmatrix}D_x\\ D_y\\ D_z\end{bmatrix}=\begin{bmatrix}0&0&0&0&e_{15}&0\\ 0&0&0&e_{24}&0&0\\ e_{31}&e_{32}&e_{33}&0&0&0\end{bmatrix}\begin{Bmatrix}\varepsilon_{xx}\\ \varepsilon_{yy}\\ \varepsilon_{zz}\\ \gamma_{yz}\\ \gamma_{xz}\\ \gamma_{xy}\end{Bmatrix}+\begin{bmatrix}\in_{11}&0&0\\ 0&\in_{22}&0\\ 0&0&\in_{33}\end{bmatrix}\begin{Bmatrix}E_x\\ E_y\\ E_z\end{Bmatrix}, \tag{7}$$

where Q_{ij} , e_{ij} and $\in_{ij}$ are elastic, piezoelectric and dielectric constants, respectively. The electric field (E_k) in terms of electric potential (Φ) is defined as follows

$$E_k=-\nabla\Phi, \tag{8}$$

where the electric potential distribution is assumed as follows (Kolahchi *et al.* 2016a)

$$\Phi(x,z,t)=-\cos\left(\frac{\pi z}{h}\right)\phi(x,t)+\frac{2V_0 z}{h}, \tag{9}$$

where V_0 is the external voltage and $\phi(x,t)$ is the electric potential dependent on x and t. However, based on SSDT (Thai and Vo 2012), Eqs. (6) and (7) can be simplified as

$$\sigma_{xx}=Q_{11}\left(\frac{\partial u}{\partial x}+z\,\frac{\partial \psi}{\partial x}\right)+e_{31}\left(\frac{\pi}{h}\sin\left(\frac{\pi z}{h}\right)\phi+\frac{2V_0}{h}\right), \tag{10}$$

$$\sigma_{xz} = Q_{55}\left(\psi + \frac{\partial w}{\partial x}\right) - e_{15}\left(\cos\left(\frac{\pi z}{h}\right)\frac{\partial \phi}{\partial x}\right), \tag{11}$$

$$D_x = e_{15}\left(\psi + \frac{\partial w}{\partial x},\right) + \in_{11}\left(\cos\left(\frac{\pi z}{h}\right)\frac{\partial \phi}{\partial x}\right), \tag{12}$$

$$D_z = e_{31}\left(\frac{\partial u}{\partial x} + z\,\frac{\partial \psi}{\partial x}\right) - \in_{33}\left(\frac{\pi}{h}\sin\left(\frac{\pi z}{h}\right)\phi + \frac{2V_0}{h}\right). \tag{13}$$

The potential energy ($U = \frac{1}{2}\int_v (\sigma_{xx}\varepsilon_{xx} + \sigma_{xc}\varepsilon_{xc} - D_x E_x)dV$) of the structure can be written as follows

$$U = \frac{1}{2}\int_V \begin{pmatrix} \sigma_{xx}\left(\frac{\partial u}{\partial x} + \frac{1}{2}\left(\frac{\partial w}{\partial x}\right)^2 + z\,\frac{\partial \psi}{\partial x}\right) \\ +\sigma_{xz}\left(\psi + \frac{\partial w}{\partial x}\right) - D_x\left(\cos\left(\frac{\pi z}{h}\right)\frac{\partial \phi}{\partial x}\right) \\ -D_z\left(-\frac{\pi}{h}\sin\left(\frac{\pi z}{h}\right)\phi - \frac{2V_0}{h}\right) \end{pmatrix} dV. \tag{14}$$

The external work (W) due to the foundation around the beams can be expressed as (Kolahchi *et al*. 2015)

$$W = \int_x \left(-k_w w + k_g \nabla^2 w\right) w dx, \tag{15}$$

where k_w and k_g respectively are spring and shear constants. However, using Hamilton's principle, the governing equations can be derived. The Hamilton's principle may be written as

$$\int_0^t (\delta U - \delta W)dt = 0, \tag{16}$$

where the variation of potential energy (δU) and variation of external work (δW) are

$$\begin{aligned} \delta U = \int_V \Bigg[& \sigma_{xx}\left(\frac{\partial \delta u}{\partial x} + \left(\frac{\partial w}{\partial x}\frac{\partial \delta w}{\partial x}\right) + z\,\frac{\partial \delta \psi}{\partial x}\right) \\ & +\sigma_{xz}\left(\psi + \frac{\partial w}{\partial x}\right) - D_x\left(\cos\left(\frac{\pi z}{h}\right)\frac{\partial \delta \phi}{\partial x}\right) \\ & -D_z\left(-\frac{\pi}{h}\sin\left(\frac{\pi z}{h}\right)\delta\phi - \frac{2V_0}{h}\right)\Bigg] dV, \end{aligned} \tag{17}$$

$$\delta W = \int_x \left(-k_w w + k_g \nabla^2 w\right)\delta w dx. \tag{18}$$

However, using Hamilton's principle and integrating by parts from the above relations, the governing equations are

$$\delta u : \frac{\partial^2 u}{\partial x^2} + \frac{\partial w}{\partial x}\frac{\partial^2 w}{\partial x^2} = 0, \tag{19}$$

$$\begin{aligned} & \delta w : -Q_{11} I\,\frac{\partial^3 w}{\partial x^3} + Q_{11} h\,\frac{\partial^2 \psi}{\partial x^2} \\ & -\left(2e_{31}V_0 + N_x^M\right)\frac{\partial^2 w}{\partial x^2} - k_w w + k_g \nabla^2 w = 0, \end{aligned} \tag{20}$$

$$\delta\psi : -Q_{11} I\,\frac{\partial^3 w}{\partial x^3} + Q_{11} h\,\frac{\partial \psi}{\partial x} - \frac{Q_{55} A}{2}\psi + \frac{e_{15} h}{2}\frac{\partial \phi}{\partial x} = 0, \tag{21}$$

$$\begin{aligned} & \delta\phi : -\frac{2h}{\pi}\frac{\partial^2 w}{\partial x^2} + \frac{h}{2}\frac{\partial \psi}{\partial x} - \frac{\pi^2 \in_{33}}{2h}\phi \\ & +\frac{h}{2}\frac{\partial \psi}{\partial x} + \frac{h \in_{11}}{2}\frac{\partial^2 \phi}{\partial x^2} = 0, \end{aligned} \tag{22}$$

In the above equations, N_x^M is the internal applied force to the beam and $I = \int z^2 dA$.

3. DQM

DQM is a numerical method that changes the differential equations to algebraic equations using weighting coefficients. Thus, at any point, it is derived as a linear sum of the weighted coefficients and values of the function at that point and other points in the direction of the axis. The main relationship of DQM can be expressed as follows (Kolahchi *et al.* 2016a, b)

$$\frac{df}{dx}\overset{x=x_i}{\rightarrow} = \sum_{j=1}^{N} C_{ij} f_j, \tag{23}$$

where $f(x)$ is a function, N is the number of grid points and C_{ij} presents weighting coefficients. The roots of the polynomial Chebyshev are heavily used in solving engineering problems and yield good results, as follows

$$X_i = \frac{L}{2}\left[1 - \cos\left(\frac{i-1}{N-1}\right)\pi\right] \quad i = 1,...,N. \tag{24}$$

The weighting coefficients are

$$C_{ij}^{(1)} = \frac{L_1(x_i)}{(x_i - x_j)L_1(x_j)} \qquad for \quad i \neq j, \quad i, j = 1,2,...,N, \tag{25}$$

$$C_{ii}^{(1)} = -\sum_{j=1, j\neq i} C_{ij}^1 \qquad for \quad i = j, \; i = 1,2,...,N, \tag{26}$$

where L_1 is a Lagrange operator that may be expressed as

$$L(x_i) = \prod_{\substack{j=1 \\ j\neq i}}^{N_x} (x_i - x_j). \tag{27}$$

And for higher derivative, we have

$$C_{ij}^{(n)} = n\left(C_{ii}^{(n-1)} C_{ij}^{(1)} - \frac{C_{ij}^{(n-1)}}{(x_i - x_j)}\right) \qquad i \neq j. \tag{28}$$

Boundary condition equations are:

- **Clamped- Clamped (CC)**

$$\begin{aligned} & w = u = \varphi = \psi = \frac{\partial w}{\partial x} = 0, \qquad at \quad x = 0 \\ & w = u = \varphi = \psi = \frac{\partial w}{\partial x} = 0. \qquad at \quad x = L \end{aligned} \tag{29}$$

- **Clamped- Simple (CS)**

$$w = u = \varphi = \psi = \frac{\partial w}{\partial x} = 0, \qquad at \quad x = 0$$
$$w = u = \varphi = \frac{\partial \psi}{\partial x} = \frac{\partial^2 w}{\partial x^2} = 0. \qquad at \quad x = L \tag{30}$$

- **Simple- Simple (SS)**

$$w = u = \varphi = \frac{\partial \psi}{\partial x} = \frac{\partial^2 w}{\partial x^2} = 0, \qquad at \quad x = 0$$
$$w = u = \varphi = \frac{\partial \psi}{\partial x} = \frac{\partial^2 w}{\partial x^2} = 0. \qquad at \quad x = L \tag{31}$$

Boundary condition equations due to having weight coefficients are coupled with governing equations. The governing equations and boundary conditions can be written in matrix form as follows

$$\left(\left[\underbrace{K_L + K_{NL}}_{K} \right] + P\left[K_g\right] \right) \begin{Bmatrix} \{d_b\} \\ \{d_d\} \end{Bmatrix} = 0, \tag{32}$$

In these relationships, P is the stability load. Also, $[K_L]$, $[K_{KL}]$ and $[K_g]$ respectively, represent the stiffness matrix linear, nonlinear part of stiffness matrix and geometric matrix. However, using the eigenvalue problem, the stability load of the structure can be obtained.

4. Numerical results

In this chapter, using the DQM, the stability load of the structure is calculated and the effect of various parameters are examined. For this purpose, a rock-soil structure made from ZnO is selected with elastic constants of Q_{11} = 207 GPa and Q_{55} =4 4.6 GPa, piezoelectric constants of e_{31} = -0.51 C/m^2 and e_{15} = -0.45 C/m^2 and dielectric constants of $\in_{11}= 7.77\times10^{-8}\ F/m$ and $\in_{33}=8.91\times10^{-8}\ F/m$. It should be noted that the stability load provided in this section, is dimensionless ($P = N_x^M / (C_{11}h)$).

Fig. 2 represents the structural stability load of the beam versus the mode number for different DQ grid points. As can be seen, with increasing the number of grid points, the stability load decreases as far as in $N = 15$, it is converged. So the calculations in the project are done with 15 grid points.

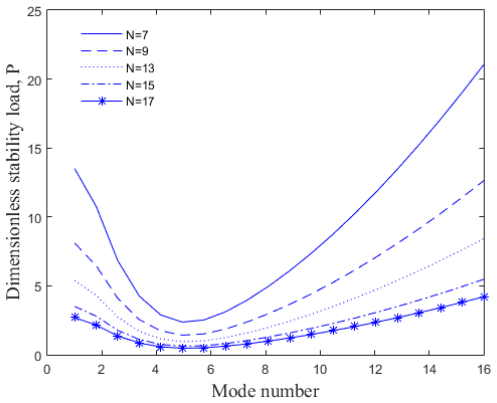

Fig. 2 Convergence and accuracy of DQM

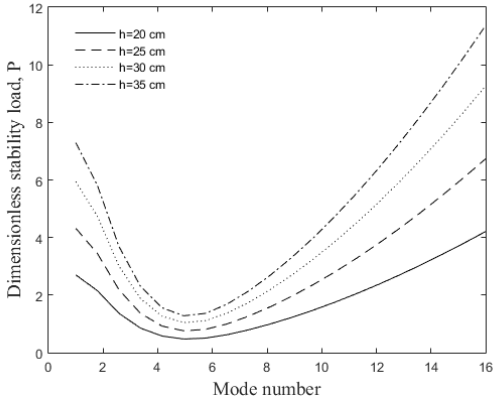

Fig. 3 Rock-soil structure thickness effect on the dimensionless stability load versus mode number

Table 1 Validation of present work with other published works

L/h	TBT, Thai (2012)	SSDT, Thai and Vo (2012)	TBT, present
5	8.9509	8.9533	8.9509
10	9.6227	9.6232	9.6227
20	9.8067	9.8068	9.8067
10	9.8671	9.8671	9.8671
0			

Stability of smart rock-soil structures has not been studied by any researcher. So to verify our results, eliminating the effects of foundation (k_w = k_g = 0) and piezoelectric properties, the stability analysis of a rock-soil structure with SSDT is discussed. Considering the material and the geometric parameters similar to Thai and Vo (2012), the stability load was shown for different aspect ratios of structure in Table 1. As can be observed, the results of the present are in accordance with reference Thai and Vo (2012) and show that the results are accurate. It should be noted that the small difference between current results and reference Thai (2012) is due to the difference in the type of theory. In this project, SSDT is used while in Thai (2012), Timoshenko rock-soil structure theory is applied.

In Fig. 3, we observe the relationship between the thickness of a rock-soil structure and its dimensionless stability load concerning the number of longitudinal modes. The point at which the stability load reaches its minimum is referred to as the critical stability load. Interestingly, this critical stability load is attained when the structure exhibits its third longitudinal mode. The underlying physical phenomenon behind this behavior lies in the impact of rock-soil structure thickness on structural stiffness. Specifically, increasing the thickness of the rock-soil structure results in an augmentation of its stiffness. Consequently, this heightened stiffness renders the rock-soil structure more resistant to stability, leading to an increase in its stability load capacity. This relationship highlights the fundamental role of material geometry in the mechanics of structural stability.

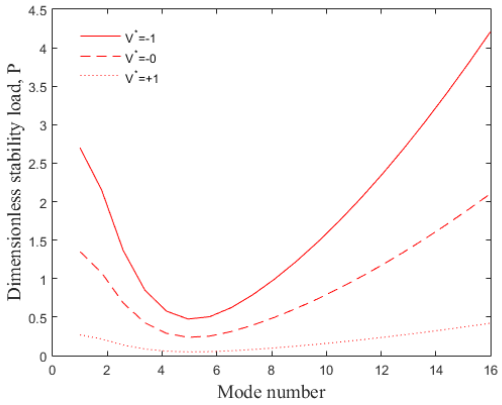

Fig. 4 External electric voltage effects on the dimensionless stability load versus mode number

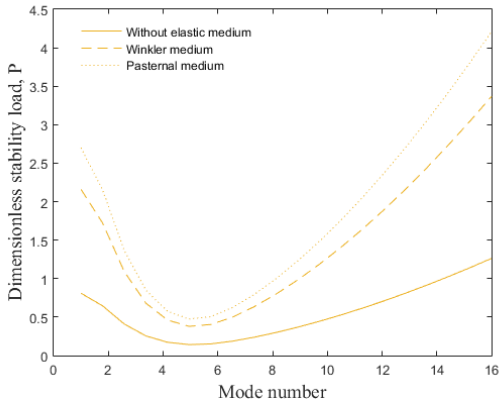

Fig. 5 Foundation effects on the dimensionless stability load versus mode number

In Fig. 4, we examine the influence of the dimensionless external applied voltage ($V^{*}=V_0/(h\sqrt{C_{11}/\in_{11}})$) on the dimensionless stability load of rock-soil structures in relation to the number of longitudinal modes. Notably, the effect of an externally applied voltage on the system is significant. When a negative external voltage is applied, it induces a compressive force within the structure, resulting in an increase in the stability load. Conversely, for positive external voltages, the effect is converse, leading to a reduction in the stability load. This observed phenomenon underscores the direct relationship between the polarity of the applied voltage and the mechanical response of the smart rock-soil structure. In summary, the application of an external voltage emerges as a potent and versatile control parameter for modulating the stability behavior of smart rock-soil structures. This physical manipulation of the electrical potential across the rock-soil structure material serves as an effective means of adjusting its structural stability, offering promising avenues for tailored engineering applications.

Fig. 5 offers insights into the influence of different types of foundations on the dimensionless stability load concerning the number of longitudinal modes. Three distinct foundation models are under consideration: a scenario without any foundation, a foundation modeled with vertical springs (Winkler model), and a foundation modeled with vertical springs along with a shear layer (Pasternak model). It is evident from the figure that the inclusion of any type of foundation leads to an increase in the stability load of the rock-soil structure compared to the structure without a foundation. This phenomenon can be explained by the fundamental principles of structural mechanics. Foundations, such as vertical springs, provide additional support to the rock-soil structure, enhancing its overall stiffness. When the stiffness of the system increases, it becomes more resistant to stability, resulting in a higher critical stability load. Furthermore, the comparison between the Winkler and Pasternak foundation models reveals an interesting distinction. The stability load of the rock-soil structure with the Pasternak foundation exceeds that of the Winkler foundation. This can be attributed to the inclusion of shear force considerations in the Pasternak model. In the

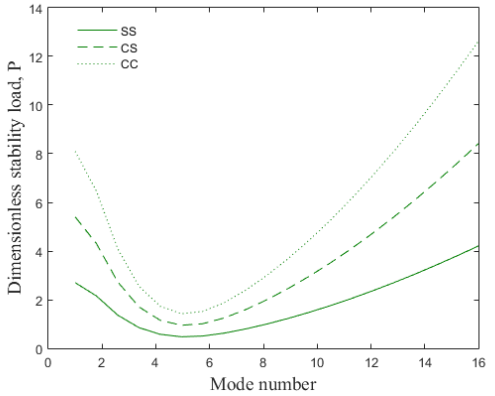

Fig. 6 Boundary condition effects on the dimensionless stability load versus mode number

Winkler model, only vertical spring elements contribute to the system's stiffness, whereas the Pasternak model incorporates both vertical springs and a shear layer. This additional consideration of shear forces further enhances the rock-soil structure's resistance to stability, thereby increasing its critical stability load. In summary, the variations in the foundation type have a substantial impact on the stability behavior of the rock-soil structure. The presence of a foundation, and especially the inclusion of shear effects in the Pasternak model, significantly contribute to the rock-soil structure's overall stability, resulting in higher stability loads. These findings underscore the importance of selecting appropriate foundation models in structural analysis and design, as they can profoundly affect the structural response and stability of the system.

Fig. 6 offers valuable insights into the impact of boundary conditions on the stability load concerning the number of longitudinal modes. Boundary conditions play a pivotal role in determining the stability and behavior of structural elements, and this figure underscores their significant influence. It is evident from the data that different boundary conditions have a substantial effect on the stability behavior of the system. In particular, when the rock-soil structure is subjected to clamped boundary conditions at both ends, it exhibits the highest stability load

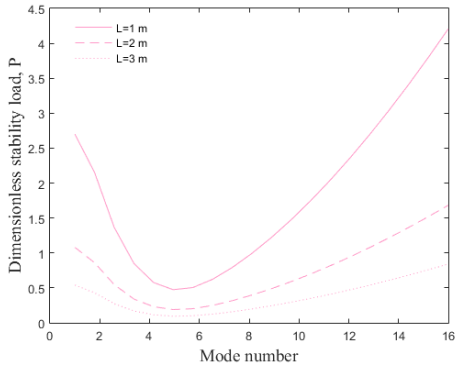

Fig. 7 The rock-soil structure length effects on the dimensionless stability load versus external electric voltage

compared to other boundary condition cases. This behavior can be comprehended through the principles of structural mechanics. Clamped boundary conditions impose a restriction on the displacement and rotation of the rock-soil structure ends, effectively "locking" them in place. As a result, the rock-soil structure experiences maximal resistance to lateral deflection or stability under compressive loads. This restriction of motion at both ends minimizes the likelihood of stability, leading to the highest critical stability load. In contrast, other boundary conditions, such as pinned or simply supported, allow varying degrees of freedom at the rock-soil structure ends, permitting lateral movement and rotation. Consequently, the stability resistance is reduced in these cases, resulting in lower critical stability loads.

In Fig. 7, we observe a clear relationship between the dimensionless stability load of a structure and the mode number for various rock-soil structure lengths. The behavior of the stability load concerning rock-soil structure length is attributed to fundamental principles of structural mechanics. The reduction in the stability load with an increase in the length of the rock-soil structure is primarily due to a decrease in the stiffness of the structure. This phenomenon can be understood through Euler's stability equation, which relates the critical stability load (P_cr) to various parameters, including the length of the rock-soil structure (L).

The equation states that as the length of the rock-soil structure increases, the critical stability load decreases, provided that other factors remain constant. The key reason for this relationship is that longer rock-soil structures tend to deflect more easily under compressive loads. As the length of the rock-soil structure increases, the potential for lateral deflection or stability also rises.

5. Conclusions

In this study, the stability of embedded smart rock-soil structures subjected to an electric field was studied. The foundation was simulated by vertical springs and shear constants. The structure was modeled by SSDT mathematically. Using the strain-displacement equations, energy method and Hamilton's principle, the coupled governing equations were derived. Finally, using DQM, the stability load of the structure was calculated and the effects of various parameters such as rock-soil structure thickness and length, external voltage and the foundation were investigated on the stability behavior of the structure. Results indicate that the critical stability load occurs in approximately the third longitudinal mode. With an increase in the rock-soil structure thickness, the stability load was increased. In general, the presence of a foundation increases the stability load of the structure. In addition, the boundary conditions have a significant effect on the rock-soil structure stability load. The results were validated with other published works.

References

Alesadi, A., Galehdari, M. and Shojaee, S. (2017), "Free vibration and stability analysis of cross-ply laminated composite plates using Carrera's unified formulation based on Isogeometric approach", *Comput. Struct.*, **183**, 38-47. https://doi.org/10.1016/j.compstruc.2017.01.013.

Benahmed, A., Fahsi, B., Benzair, A., Zidour, M., Bourada, F. and Tounsi, A. (2019), "Critical stability of functionally graded nanoscale beam with porosities using nonlocal higher-order shear deformation", *Struct. Eng. Mech.*, **69**(4), 457-466. https://doi.org/10.12989/sem.2019.69.4.457.

Bilouei, B.S., Kolahchi, R. and Bidgoli, M.R. (2018), "Stability of beams retrofitted with Nano-Fiber Reinforced Polymer (NFRP)", *Comput.*, **18**(6), 1053-106. https://doi.org/10.12989/cac.2016.18.6.1053.

Eltaher, M.A. and Mohamed, S.A. (2022), "Stability and stability analysis of sandwich beams subjected to varying axial loads", *Geomech. Eng.*, **34**(2), 241-260. https://doi.org/10.12989/gae.2022.34.2.241.

Khelifa, Z., Hadji, L., Hassaine Daouadji, T. and Bourada, M. (2018), "Stability response with stretching effect of carbon nanotube-reinforced composite beams resting on elastic foundation", *Struct. Eng. Mech.*, **67**(2), 125-130. https://doi.org/10.12989/sem.2018.67.2.125.

Kolahchi, R., Bidgoli, M.R., Beygipoor, G. and Fakhar, M.H. (2015), "A nonlocal nonlinear analysis for stability in embedded FG-SWCNT-reinforced microplates subjected to magnetic field", *J. Mech. Sci. Technol.*, **29**, 3669-3677. https://doi.org/10.1007/s12206-015-0811-9.

Kolahchi, R., Hosseini, H. and Esmailpour, M. (2016a), "Differential cubature and quadrature-Bolotin methods for dynamic stability of embedded piezoelectric nanoplates based on visco-nonlocal-piezoelasticity theories", *Compos. Struct.*, **157**, 174-186. https://doi.org/10.1016/j.compstruct.2016.08.032.

Kolahchi, R., Safari, M. and Esmailpour, M. (2016b), "Dynamic stability analysis of temperature-dependent functionally graded CNT-reinforced visco-plates resting on orthotropic elastomeric medium", *Compos. Struct.*, **150**, 255-265. https://doi.org/10.1016/j.compstruct.2016.05.023.

Mehri, M., Asadi, H. and Wang, Q. (2016), "Stability and vibration analysis of a pressurized CNT reinforced functionally graded truncated conical shell under an axial compression using HDQ method", *Comput. Method. Appl. M.*, **303**, 75-100. https://doi.org/10.1016/j.cma.2016.01.017.

Mosharrafian, F. and Kolahchi, R., (2016), "Nanotechnology, smartness and orthotropic nonhomogeneous elastic medium effects on stability of piezoelectric pipes", *Struct. Eng. Mech.*, **58**(5), 931-947. https://doi.org/10.12989/sem.2016.58.5.931.

Motezaker, M. and Eyvazian, A. (2022), "Post-stability analysis of Mindlin Cut out-plate reinforced by FG-CNTs", *Geomech. Eng.*,

34(2), 289-297. https://doi.org/10.12989/gae.2022.34.2.289.
Motezaker, M. and Eyvazian, A. (2022), "Stability load optimization of beam reinforced by nanoparticles", *Struct. Eng. Mech*., **73**(5), 481-486. https://doi.org/10.12989/sem.2022.73.5.481
Mun, S. and Cho, Y.H. (2012), "Modified harmony search optimization for constrained design problems", *Exp. Syst. Appl*., **39**, 419-423, https://doi.org/10.1016/j.eswa.2011.07.031.
Nejati, M., Eslampanah, A. and Najafizadeh, M. (2016), "Stability and vibration analysis of functionally graded carbon nanotube-reinforced beam under axial load", *Int. J. Appl. Mech.*, **8**, 1650008. https://doi.org/10.1142/S1758825116500083.
Thai, H.T. and Vo, T.P. (2012), "A nonlocal sinusoidal shear deformation beam theory with application to bending, stability, and vibration of nanobeams", *Int. J. Eng. Sci.*, **54**, 58-66. https://doi.org/10.1016/j.ijengsci.2012.01.009.
Vodenitcharova, T. and Zhang, L. (2006), "Bending and local stability of a nanocomposite beam reinforced by a single-walled carbon nanotube", *Int. J. Solids Struct.*, **43**, 3006-3024. https://doi.org/10.1016/j.ijsolstr.2005.05.014.
Yang, J., Wu, H. and Kitipornchai, S. (2017), "Stability and poststability of functionally graded multilayer graphene platelet-reinforced composite beams", *Compos. Struct.*, **161**, 111-118. https://doi.org/10.1016/j.compstruct.2016.11.048.
Yas, M. and Samadi, N. (2012), "Free vibrations and stability analysis of carbon nanotube-reinforced composite Timoshenko beams on elastic foundation", *Int. J. Press. Vess. Pip*., **98**, 119-128. https://doi.org/10.1016/j.ijpvp.2012.07.012.
Zamanian, M., Kolahchi, R. and Bidgoli, M.R. (2017), "Agglomeration effects on the stability behaviour of embedded beams reinforced with SiO2 nano-particles", *Wind. Struct.,* **24**(1), 43-57. https://doi.org/10.12989/was.2017.24.1.043.

CC